# Harmonic State Space Modeling and Analysis of Modular Multilevel Converter

Jing Lyu, Xu Cai
Wind Power Research Center
Shanghai Jiao Tong University
Shanghai, China
lvjing@sjtu.edu.cn; xucai@sjtu.edu.cn

Xin Zhang
School of Electrical and Electronic Engineering
Nanyang Technological University
Singapore
jackzhang@ntu.edu.sg

Marta Molinas
Department of Engineering Cybernetics
Norwegian University of Science and Technology
Trondheim, Norway
marta.molinas@ntnu.no

***Abstract*—Modular multilevel converter (MMC) has complex internal dynamics, such as capacitor voltage fluctuations and harmonic circulating currents, which may have a big impact on the terminal behaviors of the MMC. Therefore, it is significant to include these internal dynamics in the MMC modeling. To do this, the harmonic state space (HSS) based modeling method is applied in this work. The proposed MMC models are validated by time-domain simulations. Furthermore, the dynamic harmonic response and stability analysis of the MMC are also carried out using the harmonic transfer function (HTF).**

***Keywords—modular multilevel converter (MMC), internal dynamics, harmonic response, stability, harmonic state space (HSS), harmonic transfer function (HTF)***

## I. INTRODUCTION (*HEADING 1*)

Modular multilevel converter (MMC) has been a promising topology in medium- and high-voltage applications [1]. However, the modeling and control of the MMC becomes much more complicated than that of two-level converters [2], [3]. The MMC has complex internal dynamics, such as capacitor voltage ripples and internal circulating currents, which may have negative effects on the stability of the MMC-based power systems [4]-[6]. Therefore, different with the analysis method of the conventional converters, it is significant to include the internal dynamics when concerning the harmonic interaction and small-signal stability issues of the MMC.

In the beginning, most of the work on the MMC modeling merely focused on the external characteristics [7]-[9], e.g. ac- and dc-side V-I characteristics, while completely neglecting the internal dynamics, resulting in exactly similar models to two-level voltage source converters (VSCs). These models are feasible under the assumption that the MMC itself has enough internal damping. However, the MMC internal damping is usually weak in high-voltage applications because of the small arm resistance. Therefore, the oscillatory instability caused by the MMC internal dynamics is not able to be identified by the previous models. Recently, a few researchers have made efforts on the MMC modeling by considering internal dynamics [10]-[12]. D. Jovcic *et al*. [10] developed a small-signal dq model for the MMC based on multiple dq rotating frames, where the dc, fundamental and second harmonic were considered. Based on the same idea, the third harmonic is also considered in [11] and [12]. However, the major problems of this modeling method are the lengthy algebra as well as the difficulty to be extended to higher harmonics.

To accurately model the MMC and to readily extend to high number of harmonics for harmonic interaction studies, the harmonic state space (HSS) modeling method is first applied in this paper to model a three-phase MMC. The HSS method has already been used in many fields of power systems [13]-[15], for instance, buck-boost converters, thyristor-controlled reactors (TCRs), and two-level VSCs. However, the HSS modeling for the MMC has hardly been reported in the literature by far. This paper will present the HSS modeling of the MMC. The steady-state HSS model of the MMC is first developed, and on this basis, the small-signal dynamic HSS model is also derived. A nonlinear time-domain simulation model of a three-phase MMC is built to validate the proposed HSS models. Furthermore, the dynamic harmonic response and stability analysis of the MMC is also carried out using the harmonic transfer function (HTF).

## II. STEADY-STATE HSS MODEL OF MMC

Fig. 1 shows the averaged model of the MMC (taking one phase for instance), where $C_{arm}=C_{SM}/N$, $C_{SM}$ is the submodule (SM) capacitance, $N$ is SM number per arm, $L$ and $R$ are the arm inductance and resistance, respectively, $v_{cu}^{\Sigma}$ and $v_{cl}^{\Sigma}$ are the sum capacitor voltages of the upper and lower arms, respectively, $i_u$ and $i_l$ are the upper and lower arm currents, respectively, $v_g$ and $i_g$ are the ac-side phase voltage and current, respectively, $i_c$ is the circulating current, $n_u$ and $n_l$ are the insertion indices of the upper and lower arms, respectively, and $V_{dc}$ is the dc-side voltage. Additionally, $Z_L(=R_L+j\omega_1 L_L)$ is the ac-side R-L load determining the steady-state operating point.

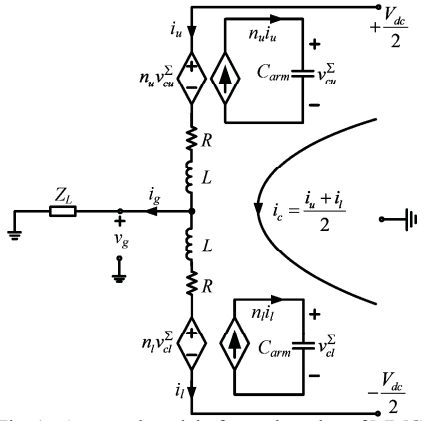

Fig. 1. Averaged model of one phase leg of MMC.

This work was supported by the National Key Research and Development Program (2016YFB0900901) and the Key Laboratory of Control of Power Transmission and Conversion of Ministry of Education (2016AC05).

978-1-5386-6054-6/18/$31.00 ©2018 IEEE

According to Fig. 1, the mathematical model of the three-phase MMC can be expressed as an LTP model like (1).

$$\dot{x}(t) = A(t)x(t) + B(t)u(t) \tag{1}$$

where the state variables and input variables are indicated as (2) and (3), respectively, and the coefficient matrices $A(t)$ and $B(t)$ are shown in the Appendix.

$$x(t) = \left[ i_{ca}, i_{cb}, i_{cc}, v_{cua}^{\Sigma}, v_{cub}^{\Sigma}, v_{cuc}^{\Sigma}, v_{cla}^{\Sigma}, v_{clb}^{\Sigma}, v_{clc}^{\Sigma}, i_{ga}, i_{gb}, i_{gc} \right]^T \tag{2}$$

$$u(t) = \left[ v_{dc} \right]^T \tag{3}$$

Hence, according to the HSS modeling procedure, the time-domain state space model in (1) can be converted into the frequency-domain HSS model, which is like

$$s\mathbf{X} = \mathbf{A}\mathbf{X} + \mathbf{B}\mathbf{U} \tag{4}$$

where $\mathbf{X}$ and $\mathbf{U}$ are shown in (5) and (6), respectively, in which the capital letters are the Fourier coefficients from [$-h$…$-1$,0,1…$h$] of each state variable, e.g. $I_{ca} = [I_{ca-h}, \cdots, I_{ca-1}, I_{ca0}, I_{ca+1}, \cdots, I_{ca+h}]$. Hence, the total number of state variables in (5) is $12\times(2h+1)$. Additionally, $\mathbf{A}$ and $\mathbf{B}$, which are doubly infinite block Toeplitz matrices of the Fourier matrix coefficients, are given in the Appendix.

$$\mathbf{X} = \left[ I_{ca}, I_{cb}, I_{cc}, V_{cua}^{\Sigma}, V_{cub}^{\Sigma}, V_{cuc}^{\Sigma}, V_{cla}^{\Sigma}, V_{clb}^{\Sigma}, V_{clc}^{\Sigma}, I_{ga}, I_{gb}, I_{gc} \right]^T \tag{5}$$

$$\mathbf{U} = \left[ V_{dc} \right]^T \tag{6}$$

By ignoring the transient item, the steady-state HSS model of the three-phase MMC can thus be obtained as

$$\mathbf{X}_{ss} = -\mathbf{A}^{-1}(\mathbf{B}\mathbf{U}) \tag{7}$$

where $\mathbf{X}_{ss}$ is the steady-state of the state variables. In addition, the dynamic response of the state variables will be discussed in the next section.

A nonlinear time-domain simulation model of a three-phase MMC has been built in MATLAB/Simulink to validate the proposed steady-state HSS model. The HSS model of the MMC is implemented using the m-file in MATLAB. An open-loop control is used and a three-phase resistor load is connected on the ac-side of the MMC. The first three harmonics are considered in the HSS model. The simulation parameters of the MMC are as follows: rated power $P_N$ = 50 MW, nominal ac line RMS voltage $V_N$ = 166 kV, nominal dc-bus voltage $V_{dc}$ = 320 kV, fundamental angular frequency $\omega_1$ = 314 rad/s, SM number per arm $N$ = 20, SM capacitance $C_{SM}$ = 140 μF, arm inductance $L$ = 360 mH, and arm resistance $R$ = 1 Ω.

As shown in Fig. 2, a good match can be observed between the steady-state HSS model and the time-domain simulation model, which shows the high accuracy of the proposed HSS model. In general case, the dc and second harmonic components are dominant in the circulating currents, and the dc, fundamental, second and third harmonic components are dominant in the capacitor voltages.

## III. Small-Signal Dynamic HSS Model of MMC

The ac voltage control for MMC is taken for example in this paper to derive the small-signal dynamic HSS model. The used ac voltage control is shown in Fig. 3, in which $H_v(s)$

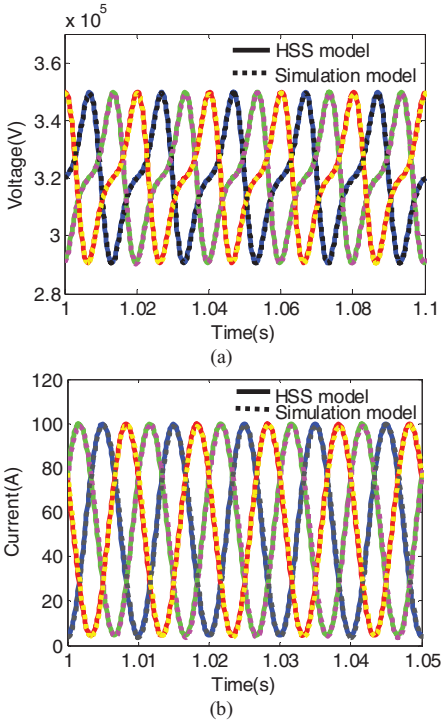


Fig. 2. Steady-state HSS model validation. (a) Three-phase upper arm capacitor voltages. (b) Three-phase circulating currents.

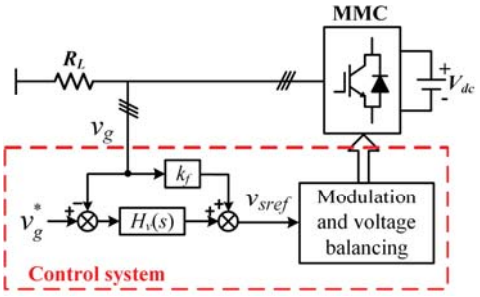


Fig. 3. AC voltage closed-loop control.

is proportional-resonant (PR) controller in order to achieve zero steady-state errors for sinusoidal quantities, and $k_f$ is the feed-forward gain to improve dynamic response.

The ac voltage regulator is

$$H_v(s) = K_p + \frac{K_r s}{s^2 + \omega_1^2} \tag{8}$$

In consideration of control dynamics, the small-signal state space model of the three-phase MMC is expressed as

$$\Delta\dot{x}(t) = A_\Delta(t)\Delta x(t) + B_\Delta(t)\Delta u(t) \tag{9}$$

where the small-signal state variables $\Delta x(t)$ and input variables $\Delta u(t)$ are shown in (10) and (11), respectively, in which $\Delta x_{PR1}$ and $\Delta x_{PR2}$ are the state variables used in the PR controller. Due to the very large scale of the coefficient matrices $A_\Delta(t)$ and $B_\Delta(t)$, they are no longer given here.

$$\begin{aligned}\Delta x(t) = \Big[ &\Delta i_{ca}, \Delta i_{cb}, \Delta i_{cc}, \Delta v_{cua}^{\Sigma}, \Delta v_{cub}^{\Sigma}, \Delta v_{cuc}^{\Sigma}, \Delta v_{cla}^{\Sigma}, \Delta v_{clb}^{\Sigma}, \Delta v_{clc}^{\Sigma}, \cdots \\ &\Delta i_{ga}, \Delta i_{gb}, \Delta i_{gc}, \Delta x_{PRa1}, \Delta x_{PRa2}, \Delta x_{PRb1}, \Delta x_{PRb2}, \Delta x_{PRc1}, \Delta x_{PRc2} \Big]^T\end{aligned} \tag{10}$$

$$\Delta u(t) = \left[ \Delta v_{dc}, \Delta v_{ga}^*, \Delta v_{gb}^*, \Delta v_{gc}^* \right]^T \tag{11}$$

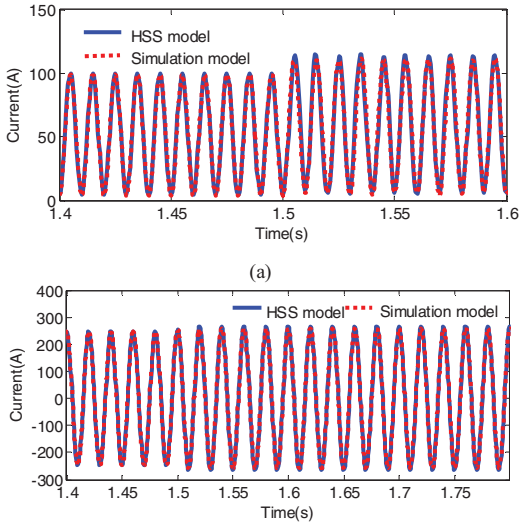


Fig. 4. Small-signal dynamic HSS model validation. (a) Phase-a circulating current. (b) Phase-a ac phase current.

By applying the HSS modeling procedure, the small-signal dynamic HSS model of the three-phase MMC can thus be obtained as

$$s\Delta\mathbf{X} = \mathbf{A}_\Delta \Delta\mathbf{X} + \mathbf{B}_\Delta \Delta\mathbf{U} \tag{12}$$

where $\Delta\mathbf{X}$, $\Delta\mathbf{U}$, $\mathbf{A}_\Delta$ and $\mathbf{B}_\Delta$ are the Fourier matrix coefficients of $\Delta x(t)$, $\Delta u(t)$, $A_\Delta(t)$, and $B_\Delta(t)$ in (9), respectively.

To validate the developed small-signal dynamic HSS model in (12), a time-domain simulation with a step change in the input variable is also carried out, from which the results are compared with those from the small-signal dynamic HSS model, as shown in Fig. 4. A step change with 10 kV fundamental voltage in the phase-a reference voltage is made at 1.5 s. It is seen that both the phase-a circulating current and ac phase current become larger after a step change in phase-a reference voltage. There is a good match between the small-signal dynamic HSS model and the time-domain simulation model.

## IV. Dynamic Harmonic Response and Stability Analysis of MMC Using HTF

The HSS model is useful for individual harmonic steady-state and dynamic analysis, which means that it is convenient to see how each individual harmonic contributes to the total response by using the HSS model.

The relationship between the dynamic harmonic coefficients of the input and output variables can be represented by the HTF, which is defined as:

$$\mathbf{H}(s) = \mathbf{C}_\Delta (s\mathbf{I} - \mathbf{A}_\Delta)^{-1} \mathbf{B}_\Delta + \mathbf{D}_\Delta \tag{13}$$

where $\mathbf{I}$ is the Toeplitz form of identity matrix, and $\mathbf{C}_\Delta$ and $\mathbf{D}_\Delta$ are the coefficient matrices of the output equation of the HSS model. Noted that $\mathbf{H}(s)$ is a double infinite matrix, as shown in (14), where it defines the coupling among different frequencies.

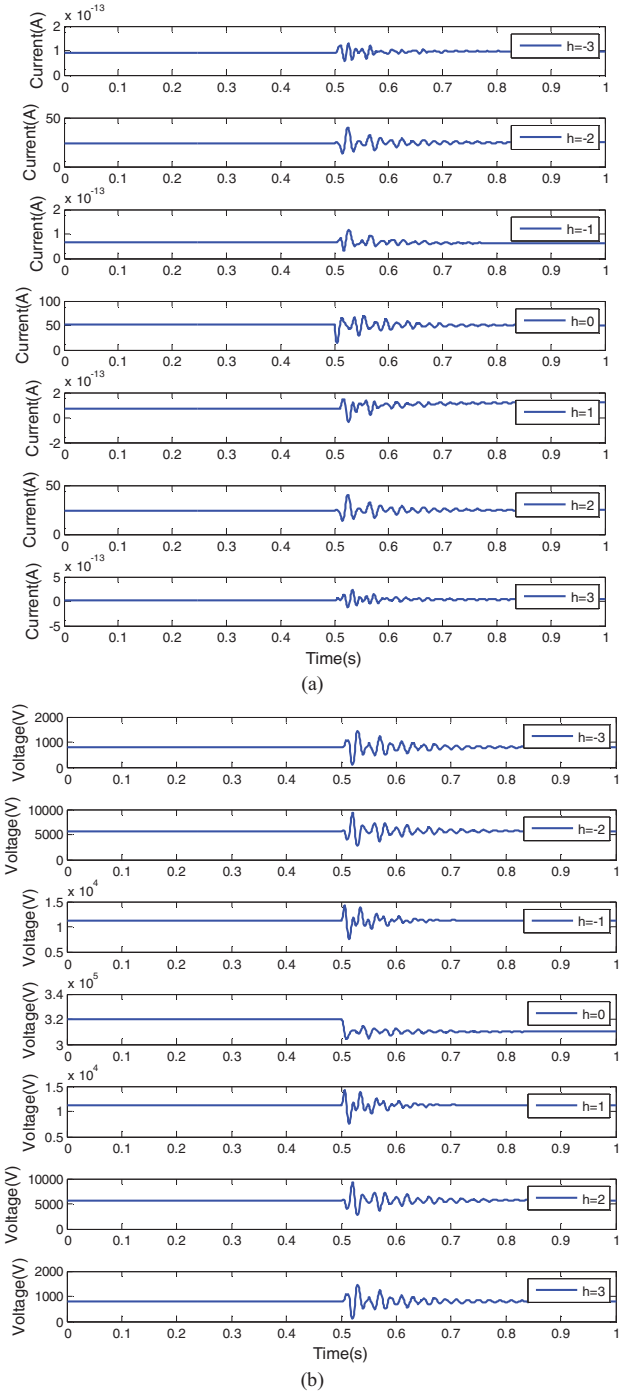


Fig. 5. Dynamic harmonic responses of the MMC from the HSS model. (a) Circulating current. (b) Upper arm capacitor voltage.

$$\mathbf{H}(s) = \begin{bmatrix} \ddots & \vdots & \vdots & \vdots & \\ \cdots & H_0(s-j\omega) & H_{-1}(s) & H_{-2}(s+j\omega) & \cdots \\ \cdots & H_1(s-j\omega) & H_0(s) & H_{-1}(s+j\omega) & \cdots \\ \cdots & H_2(s-j\omega) & H_1(s) & H_0(s+j\omega) & \cdots \\ & \vdots & \vdots & \vdots & \ddots \end{bmatrix} \tag{14}$$

Hence, the dynamic response of the individual harmonic of the output variables can be calculated by

$$\Delta\mathbf{Y} \overset{\mathbf{C}_\Delta=\mathbf{I},\mathbf{D}_\Delta=\mathbf{O}}{=} \Delta\mathbf{X} = \mathbf{H}(s)\Delta\mathbf{U} \tag{15}$$

It is pointed out that the harmonic response obtained from (15) is the output harmonic vector in $s$-domain, which needs to be converted to the time-domain response by using

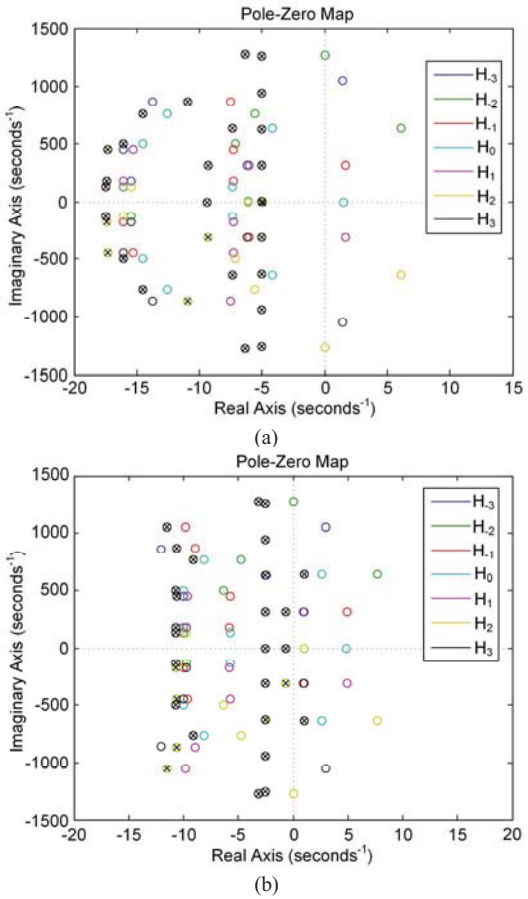


Fig. 6. Pole-zero mapping of the HTF of the MMC. (a) $K_p$=1. (b) $K_p$=2.

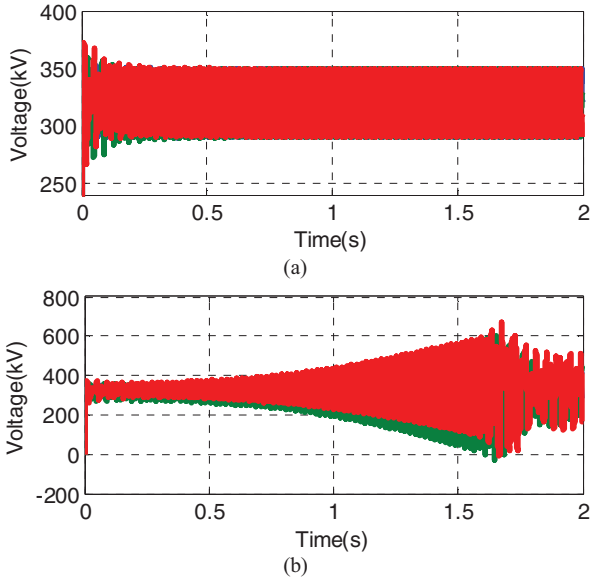


Fig. 7. Time-domain simulation results. (a) $K_p$=1. (b) $K_p$=2.

the inverse Laplace transform. Furthermore, the final response is obtained by adding the steady-state and dynamic responses.

The time responses of each harmonic of the circulating current and capacitor voltage are depicted in Fig. 5, where a 10 kV step change in the dc-bus voltage happens at 0.5 s. For simplification of analysis, -3$^{rd}$-3$^{rd}$ harmonics of the HSS model are considered. It is observed that the circulating current contains dc and second harmonic components, as seen in Fig. 5(a), where the amplitudes at the fundamental-frequency and third harmonic are near zero ($10^{-13}$). Furthermore, the capacitor voltage contains dc and all harmonic components, as shown in Fig. 5(b). In addition, it is also seen that there exist large overshoots and slow dynamic responses in each harmonic during the dynamic process, which is mainly due to the weak internal damping within the MMC.

The stability of the MMC system can also be assessed by the HTF, where the contribution of each harmonic to the system instability can be explicitly identified. Fig. 6 depicts the pole-zero mapping of the HTF of the MMC, where the HTF describes the relationship between each harmonic of $\Delta I_{ga}$ and $\Delta V_{ga}^{*}$. Fig. 6(a) shows the stable case where the proportional gain of the ac voltage controller is $K_p$ = 1, while Fig. 6(b) shows the unstable case where the proportional gain is $K_p$ = 2. It can be seen that the instability of the MMC in this case is mainly attributed to the third harmonic capacitor voltage dynamic. The time-domain simulation results are also demonstrated to validate the theoretical analysis, as shown in Fig. 7, where the three-phase upper arm sum voltages of the MMC are presented. In the time-domain simulation, the MMC system becomes unstable when the proportional gain of the ac voltage controller changes from 1 to 2, which confirms the theoretical analysis.

## V. Conclusion

This paper investigated the harmonic state space (HSS) modeling of the MMC. The steady-state and small-signal dynamic HSS models of the MMC have been developed in this paper, respectively. The results show that the proposed HSS models are able to represent all harmonics in capacitor voltages and circulating currents. Moreover, the proposed HSS models are easily extended to any high harmonics. In addition, the dynamic response of each harmonic of the MMC as well as its contribution to the system stability can be readily identified by the harmonic transfer function (HTF).

## References


[1] M. A. Perez, S. Bernet, J. Rodriguez, S. Kouro, and R. Lizana, "Circuit topologies, modeling, control schemes, and applications of modular multilevel converter," *IEEE Trans. Power Electron.*, vol. 30, no. 1, pp. 4-17, 2015.

[2] K. Ilves, A. Antonopoulos, S. Norrga, and H.P. Nee, "Steady-state analysis of interaction between harmonic components of arm and line quantities of modular multilevel converters," *IEEE Trans. Power Electron.*, vol. 27, no. 1, pp. 57-68, 2012.

[3] F. Deng and Z. Chen, "A control method for voltage balancing in modular multilevel converters," *IEEE Trans. Power Electron.*, vol. 29, no. 1, pp. 66-76, 2014.

[4] J. Lyu, X. Cai, M. Amin, and M. Molinas, "Subsynchronous oscillation mechanism and its suppression in MMC-Based HVDC connected wind farms," *IET Generation, Transmission & Distribution*, vol. 12, no. 4, pp. 1021-1029, 2018.

[5] J. Lyu, X. Cai, and M. Molinas, "Frequency domain stability analysis of MMC-based HVdc for wind farm integration," *IEEE Journal of Emerging and Selected Topics in Power Electronics*, vol. 4, no. 1, pp. 141-151, 2016.

[6] J. Lyu, X. Cai, and M. Molinas, "Optimal design of controller parameters for improving the stability of MMC-HVDC for wind farm integration," *IEEE Journal of Emerging and Selected Topics in Power Electronics*, vol. 6, no. 1, pp. 40-53, 2018.

[7] G. Bergna, J. A. Suul, and S. D'Arco, "Small-signal state-space modeling of modular multilevel converters for system stability analysis," in *Proc. IEEE ECCE*, 2015, pp. 5822-5829.

[8] N. T. Trinh, M. Zeller, K. Wuerflinger, and I. Erlich, "Generic model of MMC-VSC-HVDC for interaction study with ac power system," *IEEE Trans. Power Syst.*, vol. 31, no.1, pp. 27-34, 2016.

[9] H. Saad, J. Mahseredjian, S. Dennetiere, and S. Nguefeu, "Interactions studies of HVDC-MMC link embedded in an AC grid," *Electr. Power Syst. Res.*, vol. 138, pp. 202-209, 2016.

[10] G. Bergna, J. A. Suul, and S. D'Arco, "State-space modelling of modular multilevel converters for constant variables in steady-state," in *Proc. IEEE COMPEL*, 2016, pp. 1-9.

[11] T. Li, A. M. Gole, and C. Zhao, "Harmonic instability in MMC-HVDC converters resulting from internal dynamics," *IEEE Trans. Power Del.*, vol. 31, no. 4, pp. 1738-1747, 2016.

[12] A. Jamshidifar and D. Jovcic, "Small-signal dynamic DQ model of modular multilevel converter for system studies," *IEEE Trans. Power Del.*, vol. 31, no. 1, pp. 191-199, 2016.

[13] G. N. Love and A. R. Wood, "Harmonic state space model of power electronics," in *Proc. Int. Conf. Harmonics Quality of Power*, Wollongong, Australia, 2008, pp. 1-6.

[14] J. R. C. Orillaza and A. R. Wood, "Harmonic state-space model of a controlled TCR," *IEEE Trans. Power Del.*, vol. 28, no. 1, pp. 197-205, 2013.

[15] J. Kwon, X. Wang, F. Blaabjerg, C. L. Bak, V. S. Sularea, and C. Busca, "Harmonic interaction analysis in a grid-connected converter using harmonic state space (HSS) modeling," *IEEE Trans. Power Electron.*, vol. 32, no. 9, pp. 6823-6835, 2017.

## APPENDIX

The coefficient matrices in (1) and (4) are shown in (A1)-(A4), in which $\Gamma[\ ]$ means the Toeplitz matrix of the Fourier coefficients of the time varying variables, $I$ is identity matrix, $O$ is zero matrix. Additionally, the lowercase letters in (A1) denote the time-domain signals, and the uppercase letters in (A3) represent the Fourier coefficients from [-$h$… -1,0,1… $h$]. And $Q$ is a diagonal matrix that represents the frequency information, which is like (A5).

$$A(t)=\begin{bmatrix}
-\frac{R}{L} & 0 & 0 & -\frac{n_{ua}}{2L} & 0 & 0 & -\frac{n_{la}}{2L} & 0 & 0 & 0 & 0 & 0 \\
0 & -\frac{R}{L} & 0 & 0 & -\frac{n_{ub}}{2L} & 0 & 0 & -\frac{n_{lb}}{2L} & 0 & 0 & 0 & 0 \\
0 & 0 & -\frac{R}{L} & 0 & 0 & -\frac{n_{uc}}{2L} & 0 & 0 & -\frac{n_{lc}}{2L} & 0 & 0 & 0 \\
\frac{n_{ua}}{C_{arm}} & 0 & 0 & 0 & 0 & 0 & 0 & 0 & 0 & \frac{n_{ua}}{2C_{arm}} & 0 & 0 \\
0 & \frac{n_{ub}}{C_{arm}} & 0 & 0 & 0 & 0 & 0 & 0 & 0 & 0 & \frac{n_{ub}}{2C_{arm}} & 0 \\
0 & 0 & \frac{n_{uc}}{C_{arm}} & 0 & 0 & 0 & 0 & 0 & 0 & 0 & 0 & \frac{n_{uc}}{2C_{arm}} \\
\frac{n_{la}}{C_{arm}} & 0 & 0 & 0 & 0 & 0 & 0 & 0 & 0 & -\frac{n_{la}}{2C_{arm}} & 0 & 0 \\
0 & \frac{n_{lb}}{C_{arm}} & 0 & 0 & 0 & 0 & 0 & 0 & 0 & 0 & -\frac{n_{lb}}{2C_{arm}} & 0 \\
0 & 0 & \frac{n_{lc}}{C_{arm}} & 0 & 0 & 0 & 0 & 0 & 0 & 0 & 0 & -\frac{n_{lc}}{2C_{arm}} \\
0 & 0 & 0 & -\frac{n_{ua}}{L} & 0 & 0 & \frac{n_{la}}{L} & 0 & 0 & -\frac{R+2Z_L}{L} & 0 & 0 \\
0 & 0 & 0 & 0 & -\frac{n_{ub}}{L} & 0 & 0 & \frac{n_{lb}}{L} & 0 & 0 & -\frac{R+2Z_L}{L} & 0 \\
0 & 0 & 0 & 0 & 0 & -\frac{n_{uc}}{L} & 0 & 0 & \frac{n_{lc}}{L} & 0 & 0 & -\frac{R+2Z_L}{L}
\end{bmatrix} \tag{A1}$$

$$B(t)=\left[\frac{1}{2L},\frac{1}{2L},\frac{1}{2L},0,0,0,0,0,0,0,0,0\right]^T \tag{A2}$$

$$\mathbf{A}=\begin{bmatrix}
-\frac{R}{L}I-Q & O & O & -\frac{\Gamma[N_{ua}]}{2L} & O & O & -\frac{\Gamma[N_{la}]}{2L} & O & O & O & O & O \\
O & -\frac{R}{L}I-Q & O & O & -\frac{\Gamma[N_{ub}]}{2L} & O & O & -\frac{\Gamma[N_{lb}]}{2L} & O & O & O & O \\
O & O & -\frac{R}{L}I-Q & O & O & -\frac{\Gamma[N_{uc}]}{2L} & O & O & -\frac{\Gamma[N_{lc}]}{2L} & O & O & O \\
\frac{\Gamma[N_{ua}]}{C_{arm}} & O & O & -Q & O & O & O & O & O & \frac{\Gamma[N_{ua}]}{2C_{arm}} & O & O \\
O & \frac{\Gamma[N_{ub}]}{C_{arm}} & O & O & -Q & O & O & O & O & O & \frac{\Gamma[N_{ub}]}{2C_{arm}} & O \\
O & O & \frac{\Gamma[N_{uc}]}{C_{arm}} & O & O & -Q & O & O & O & O & O & \frac{\Gamma[N_{uc}]}{2C_{arm}} \\
\frac{\Gamma[N_{la}]}{C_{arm}} & O & O & O & O & O & -Q & O & O & -\frac{\Gamma[N_{la}]}{2C_{arm}} & O & O \\
O & \frac{\Gamma[N_{lb}]}{C_{arm}} & O & O & O & O & O & -Q & O & O & -\frac{\Gamma[N_{lb}]}{2C_{arm}} & O \\
O & O & \frac{\Gamma[N_{lc}]}{C_{arm}} & O & O & O & O & O & -Q & O & O & -\frac{\Gamma[N_{lc}]}{2C_{arm}} \\
O & O & O & -\frac{\Gamma[N_{ua}]}{L} & O & O & \frac{\Gamma[N_{la}]}{L} & O & O & -\frac{R+2Z_L}{L}I-Q & O & O \\
O & O & O & O & -\frac{\Gamma[N_{ub}]}{L} & O & O & \frac{\Gamma[N_{lb}]}{L} & O & O & -\frac{R+2Z_L}{L}I-Q & O \\
O & O & O & O & O & -\frac{\Gamma[N_{uc}]}{L} & O & O & \frac{\Gamma[N_{lc}]}{L} & O & O & -\frac{R+2Z_L}{L}I-Q
\end{bmatrix} \tag{A3}$$

$$\mathbf{B}=\left[\frac{1}{2L}I,\frac{1}{2L}I,\frac{1}{2L}I,O,O,O,O,O,O,O,O,O\right]^T \tag{A4}$$

$$Q=\mathrm{diag}\left[-jh\omega_1,\cdots,-j\omega_1,0,j\omega_1,\cdots,jh\omega_1\right] \tag{A5}$$